ORIGINAL RESEARCH

Biomass gasification in a double-tapered bubbling fluidized bed reactor using preheated air

Gokul Gopan[1] · Lalhmingsanga Hauchhum[1] · Pankaj Kalita[2] · Satyajit Pattanayak[1]

Abstract

Production of clean energy from biomass through thermochemical conversion techniques has gained substantial momentum over the last decades. The biomass gasification is a noteworthy thermochemical conversion technique due to its varied advantages like feed material flexibility and ease of operation. Here in this work, the effects of applying air preheating for the gasification of biomass (dry wood) under varied particle size (100, 300 and 800 μm) and its outcome are simulated using ANSYS FLUENT 14.0. Two-fluid model is used for the simulation study with distinct phases—air (Phase-1) and wood (Phase-2). The boundary conditions are applied, and the simulation results obtained are matched with available studies. The inlet velocity of the gasifying medium is varied from 0-3m/s analogous to the bubbling fluidized bed velocity range. The gasification temperature ranges are 973, 1073 and 1173 K. The simulations are conducted with and without preheated air in a double-tapered bubbling fluidized bed reactor having taper angle of 5°.The fluid velocity and taper angle play an essential role in controlling the solid particle suspension rate inside the reactor chamber. However, the air preheating maintains the overall reactor temperature that enhances the solid–gas conversion rate.

Keywords Double-tapered bubbling fluidized bed reactor · Taper angle · Biomass gasification · Air preheating · Energy conversion techniques · Computational fluid dynamics

Abbreviations

CFD	Computational fluid dynamics
DTBFBR	Double tapered bubbling fluidized bed reactor
PCFB	Pressurised circulating fluidized bed
g	Acceleration due to gravity (ms^{-2})
H_g	Specific enthalpy of gas (kJ/kg)
∇	Gradient operator
T	Mean temperature (K)
k_i	Turbulent kinetic energy (m^2s^{-2}) of species i
$\vec{v}_S$	Solid fluctuation velocity (m/s)
$\vec{v}_g$	Gas fluctuation velocity (m/s)
S	Source term for heat released
g	Gas phase
S	Solid phase
εo	Fixed bed voidage (-)
ρ_{sus}	Suspension density (kgm^{-3})
ρ_s	Solid density (kgm^{-3})
ρ_g	Gas density (kgm^{-3})
P_g	Gas phase pressure
$\underline{P_s}$	Solid phase pressure
$\overline{\overline{\tau_g}}$	Gas phase stress tensor
$\overline{\overline{\tau_s}}$	Solid phase stress tensor
dp	Particle diameter
ε	Volume fraction
C	Carbon
O_2	Oxygen
H	Hydrogen
CH_4	Methane
CO_2	Carbon dioxide
CO	Carbon monoxide
H_2O	Water

✉ Gokul Gopan
  gokul.mech@nitmz.ac.in

1   Department of Mechanical Engineering, National Institute of Technology Mizoram, Mizoram 796012, India

2   Centre for Energy, Indian Institute of Technology Guwahati, Assam 781039, India

Introduction

The present world is seeking endless inventions and technological development that always expects novelty and optimization. The renewable energy production technique is prominent among them. The fossil fuel resources utilized

presently are dug from the earth which has undergone thermochemical conversions for many thousands of years under significant temperature, pressure and other factors. Studies and simulations are always performed to accelerate such thermochemical activities to overcome any associated issues with a fuel shortage and safe environment without greenhouse gases [1]. Hence, the production of clean energy is of paramount importance. Energy production from biomass sources through thermochemical conversion techniques has gained substantial momentum over the last decades [2]. Though various thermochemical conversion methods (pyrolysis, combustion and liquefaction) are available, gasification has gained vital importance in recent years due to its worthy advantages [3]. The gasification technique ensures flexibility in adopting any kind of biomass feedstock for producing chemicals, generating electric power and high-value engine fuels [4]. Gasification involves the partial oxidation of feedstocks with homogenous or heterogeneous particle size under suitable operating conditions to produce non-condensable gas mixture like CO, CO_2, H_2, CH_4 and other gaseous products in a reactor [5, 6]. Various types of reactors like fixed bed, downdraft, circulating fluidized bed, bubbling fluidized bed are used in mega and large industries for dedicated power production needs [7].

The performance comparison of tapered fluidized bed reactor with varied taper angles is conducted by Sau. et al. [8]. He compared tapered fluidized bed reactor with conventional cylindrical-shaped reactors and found that the improvement in particle suspension density at the diverging section of the reactor due to velocity gradient of the gasifying medium enhanced the solid–gas conversion rate and fluidization behaviour. However, more accurate study and development on hydrodynamics of tapered fluidized bed are reported by Rasteh et al. [9]. They used particles belonging to Geldart B classification and concluded that the particle hydrodynamics depend on operating conditions, geometrical constraints of the particle, reactor bed (bottom region) dimensions and density of the fluidizing agent. Moreover, considering the interparticle forces and initial stagnant bed height will also improve the overall process. The work conducted by Schulzke. T [10] reported that preheating the gasifying agent improves the adiabatic flame temperature; however, as the general solid conversion reactions are exothermic, that reduces the biomass content; improving the operating pressure will have the upper hand on maintaining thermal equilibrium [11]. On the contrary, preheating the gasifying agent helps to reduce the moisture content [12] of biomass feedstock further and maintain the temperature required inside the reactor [13].

The syngas produced during biomass gasification is very versatile, and its quality is determined by operating parameters like gasifying medium, optimum equivalence ratio and reaction temperature [14–16]. However, the chemical reactions occurring during gasification process are independent of the gasifier design. The producer gas composition alters at higher temperatures. The percentage composition of H_2 and CO is increased at higher temperatures (>1273 K) with a simultaneous reduction in CH_4, CO_2 and H_2O; however, the presence of nitrogen in the air slows down the conversion reaction [17]. The presence of moisture content reduces the overall producer gas composition [18]. The percentage composition of methane in the producer gas is found to be 2-4%, between the temperature ranges 673–873 K [19–21]. Flue gasses or effluent from any combustion process relieves greenhouse gasses that cannot be eliminated but could be reduced. Studies conducted by Kalita et al [22–24], in pressurized circulating fluidized bed (PCFB) reactor with various biomasses, sand blend percentages under high pressure and superficial velocity, have shown increased heat transfer coefficient; however, maximum heat transfer is obtained at 12.5% sand blend with biomass above which the heat transfer coefficient is diminished with increased superficial velocity.

In this work, the gasification of wood biomass under varied particle size, temperature and air (gasifying medium) velocity with multiphase Eulerian model is discussed. The variation of particle hydrodynamics and specific operating parameters with the varying reactor taper angles has not been discussed in published studies hitherto. However, the experiments and simulation on gasification process that yields various syngas constituents have not been conducted which otherwise will enhance the significance of this work. Hence, the present work discusses purely the uniqueness of tapered reactor with taper angle of 5°. The Eulerian/two-fluid models treat the solid–gas interface as an interpenetrating continuum which predicts the fluidic behaviour more precisely [25].

The bubbling fluidized bed set-up is adopted for the study having a double-tapered reactor with taper angle of 5°. The bubbling fluidized bed reactors are beneficial in terms of simpler construction, good heat transfer and storage and use of lesser particle sized materials (<3mm) compared to other costly reactor systems [3, 26] The double-tapered bubbling fluidized bed reactor (DTBFBR) shape is novel, self-designed, following the pieces of the literature that have successfully highlighted the performance dissimilarities matched to conventional columnar reactors where different taper angles (4.61°, 7.47° and 9.52°) are adopted for tapered-in reactors [27–29]. The bed pressure drop in a tapered-in, tapered-out fluidized bed reactor with taper angle 4.6° increases with the initial bed height, whereas for smaller bed height, the fractional conversion is increased to maximum and then decreases with the increase in bed height [30]. The solid particle adhesion on the inner walls of cylindrical reactor during combustion reduces the reactor efficiency, which is a noteworthy observation obtained from the

published data. However, the novel tapered shape of reactor helps the solid particle to escape along the side walls without agglomeration and enhances the solid circulation due to the increased cross-sectional area. As the scope of this work is to understand the effects in utility of preheated air during gasification, the molar concentration of exit gas (syngas), devolatilization and particle cluster formation remains the part of forthcoming computational analysis work.
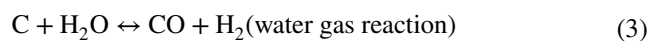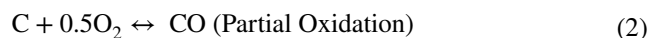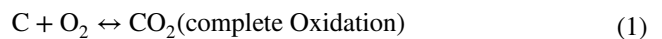
Materials and methods

The present work focuses only on the computational modelling of the gasification process in a DTBFBR. Hence, the experiment details are not presented and it remains as the part of future work. The simulations are conducted with and without injection of preheated air (333K) to understand the potential advantages of biomass preheating. The variation of temperature, pressure drop and volume fraction for different particle sizes is studied separately for gas phase and solid phase.

The DTBFBR set-up comprises of a double-tapered fluidized bed reactor having taper angle 5° as shown in Fig. 1. The biomass material (wood) is fed through the biomass feeder. The gasifying medium (air) pumped from the blower at different velocities fluidizes the wood biomass and drags towards the exit. The U-tube manometer records the pressure drop produced by the gasifying medium. Biomass

gasification is a self-sustaining process [31]. Hence, the inclusion of external electric heater is to impart the heating required for the combustion of biomass. The syngas produced after the combustion of particles leaves through the reactor exit. Gas and solid particles are separated through a cyclone separator. The particulate collector collects the unburnt solid ash particles, and syngas will be collected through the syngas exit. The hydrodynamic features in a DTBFBR largely depend on the particle sphericity, density, viscous nature of the gasifying medium, adhesive interparticle forces, reactor taper angles, stagnant bed height, etc. [9, 32]. Gasification of biomass involves chemical reactions that are happening at different temperatures. In general, drying (0–200°), pyrolysis (200–500°) and gasification (700–900°) occur at these temperatures, which may vary with the type and size of the reactor [33]. The major chemical reactions taking place during gasification in 2 stages adopted from various studies are as follows [34–36].

Stage 1

$$C + O_2 \leftrightarrow CO_2 (\text{complete Oxidation}) \tag{1}$$

$$C + 0.5O_2 \leftrightarrow CO \ (\text{Partial Oxidation}) \tag{2}$$

$$C + H_2O \leftrightarrow CO + H_2 (\text{water gas reaction}) \tag{3}$$

Stage 2
Water gas mixture shift reaction

Fig. 1 DTBFBR set-up for gasification **a** blower, **b** thermocouple-1, **c** DTBFBR with taper angle 5°, **d** thermocouple-2, **e** particulate collector, **f** cyclone separator, **g** syngas exit, **h** heater coil (outer), **i** biomass feed, **j** U-Tube manometer, **k** air preheater

$$CO + 3H_2 \leftrightarrow CH_4 + H_2O \ (\text{Methanation}) \qquad (4)$$

$$CO + H_2O \leftrightarrow CO_2 + H_2 \qquad (5)$$
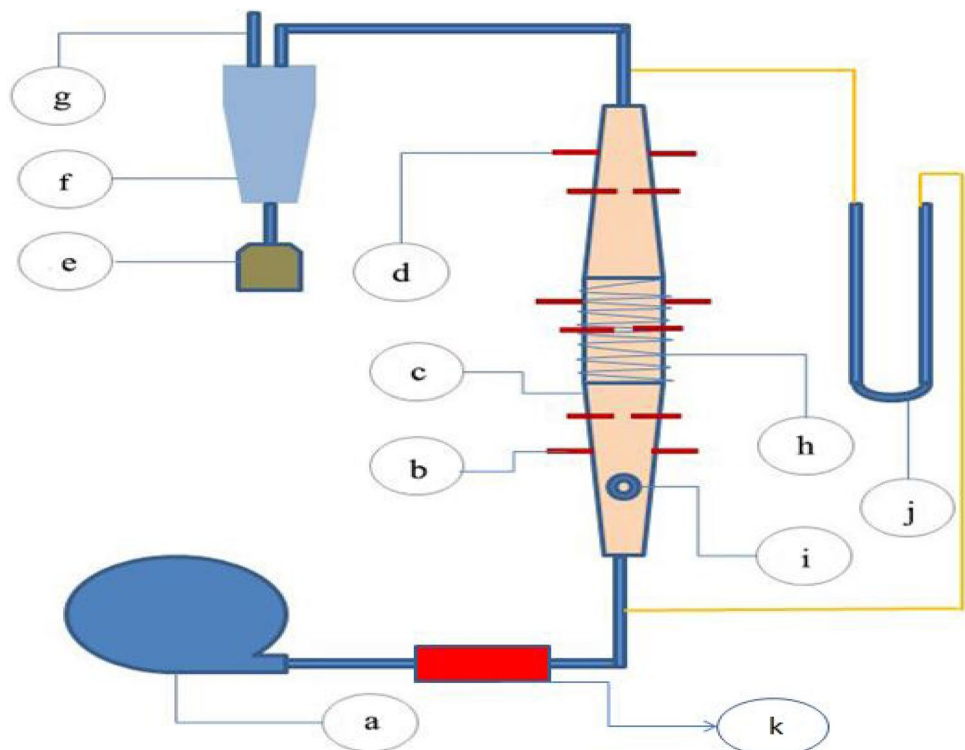
here in equations, only Eq. 3 is endothermic, the moisture content present in the biomass will be readily evaporated to produce the products H_2 and CO. Rest all other chemical reactions [Eqs. 1 , 2, 4 , 5] involve the liberation of heat energy.

Computational modelling

Computational modelling of any real scenario represents the exact operating environment, but the results cannot be presumed to be accurate. However, the computational and numerical calculations inflict on the limits of process optimization. In this particular work, certain assumptions are made during the process simulation. The reactor is assumed to be operating under uniform temperature and fluid velocity. The boundary conditions and computational modelling details are enlisted in Tables 1 and 2. The solid biomass material is considered to be fed intermittently in sufficient quantities rather than continuous mass flow rate. The details of wood biomass are given in Table 2. The equivalence ratio and stoichiometry are not considered since the gasifying medium is purely adopted as air from the material database. The 2D computational modelling is accomplished using ANSYS Fluent Solver 14.5. The DTBFBR geometry is created with an axial reactor height of 1.20m, reactor inlet and exit diameter of 0.10 m each. The heating zone is located in the middle section precisely at the centre with 0.10 m length in either direction.

Table 2 Computational modelling details of the DTBFBR

Reactor top diameter (m)	0.10
Reactor bottom diameter (m)	0.10
Total height of reactor (m)	1.2
Reactor wall thickness (m)	0.006
Bed height (wood biomass) (m)	0.20
Gas velocity (air) at inlet (m/s)	1,2,3
Gas density (air)(kg/ m^3)	1.225
Solid density(wood biomass) (kg/m^3)	1400
Thermal conductivity (wood biomass)(W/ mK)	0.32
Initial solid packing	0.63
Particle diameter, spherical (μm)	100,300,800
DTBFBR material	Steel
Solver type	Pressure based
Simulation type (time)	Transient
Gravity (m/s^2)	– 9.81 (Y-direction)
Solution model	Multiphase Eulerian
Solution scheme	Phase-coupled SIMPLE
Solution initialization	Standard (inlet)
Viscous model	Laminar
Time step (s)	0.001
Number of time steps	3000

The geometry domain with 2752 elements having element size of 0.00625 is selected as the independent parameter for simulation as given in Table 3 because the average orthogonal quality is 0.8 and the elemental quality is between the limits of 0-1. This means that better simulation accuracy will be obtained with the selected element size. The Y-plus value is obtained from the XY plot for transient flow with 1m/s inlet velocity. P_1, P_2 and ΔP are the pressure values at the inlet, outlet and pressure drop,

Table 1 Boundary conditions used for simulation

Description	Type
Inlet	Velocity inlet
	Mixture pressure-101325Pa
	Primary Phase-1 (air)-1,2,3m/s
	Temperature-300K
	Secondary Phase-2 (wood biomass)
	Volume fraction-1
	Temperature-300K
Heating Zone (wall)	Temperature of Phase-1-973K, 1073K, 1173K, Phase-2-973K, 1073K, 1173K
Wall	Stationary wall, no slip for gas phase, No shear for solid phase
	Material–cast iron
	Thermal mixed with Conduction and convection
	Wall Thickness-0.006m
	Free stream temperature-300K
Outlet	Pressure outlet, conditions not defined

Table 3 Mesh independence parameters

Sl. no	Element size	Number of elements	Y-plus value	P_1	P_2	ΔP
1	0.05	44	110	0.135968	0.131432	0.004536
2	0.025	176	58	0.164285	0.105196	0.059089
3	0.0125	688	0.01	0.191789	0.124011	0.067778
4	0.00625	2752	15	0.213727	0.146327	0.0674
5	0.003125	11008	10.1	0.225409	0.154819	0.07059
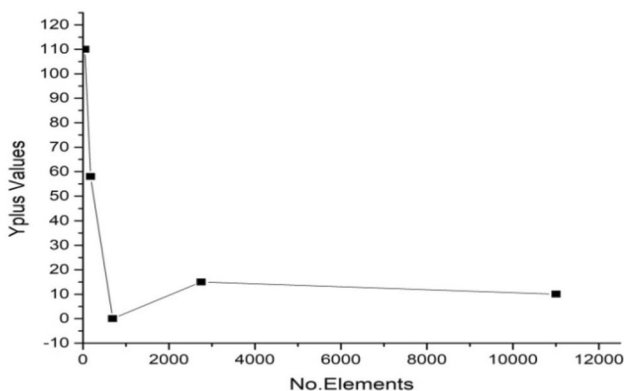
Fig. 2 Plot for mesh independence test with Y-plus values and number of elements

respectively. The Y-plus value for a different number of mesh elements is plotted in Fig. 2. The element size of 0.00625 is considered most suitable for the current simulation when compared with other element sizes due to lower element size and number of elements that saves computational time. The mesh method used is automatic with tetrahedron cells. The solution set-up proceeds by defining the gas–solid phases (interpenetrating) where Phase-1 is the air and Phase-2 is the wood biomass. Phase interaction follows Gidaspow drag model with mass transfer from Phase-2 to Phase-1. The species transport with chemical reaction to find the molar concentration of outlet gaseous constituents is not included in this work and remains to be part of future work. The quantity of biomass fed to the reactor is calculated using bed height. Hence, the volume fraction of Phase-2 at the inlet is patched to 1 up to the bed height of 0.20 m. The temperature and pressure at the inlet for Phase-1 and Phase-2 are set to 300 K and 101325 Pa for all simulation runs except the preheating. The inlet velocity, temperature and particle size are varied for each simulation run with necessary boundary condition, and results are obtained. Solution scheme used is phase-coupled simple and first-order upwind for momentum exchange. Transient simulation is followed with a time step size of 0.001 and time steps 6000. The results are considered only till 3000-time step since most of the input biomass left the reactor during the gasification process.

Model equations

Computational fluid dynamic simulations explicitly solve momentum, mass and energy equations of gas–solid phase in a DTBFBR using finite volume approach through Eqs. 6, 7, 8, 9 and 10.

$$\frac{\partial}{\partial_t}\left(\varepsilon_g \rho_g\right) + \nabla.\left(\varepsilon_g \rho_g \vec{v}_g\right) = 0 \tag{6}$$

$$\frac{\partial}{\partial_t}\left(\varepsilon_s \rho_s\right) + \nabla.\left(\varepsilon_s \rho_s \vec{v}_s\right) = 0 \tag{7}$$

Continuity equation (gas phase and solid phase) [37]

$$\frac{\partial}{\partial_t}\left(\varepsilon_g \rho_g \vec{v}_g\right) + \nabla.\left(\varepsilon_g \rho_g \vec{v}_g \vec{v}_g\right) = -\varepsilon_g \nabla.P_g + \nabla.\overline{\overline{\tau_g}} + \varepsilon_g \rho_g \vec{g} \tag{8}$$

$$\frac{\partial}{\partial_t}\left(\varepsilon_s \rho_s \vec{v}_s\right) + \nabla.\left(\varepsilon_s \rho_s \vec{v}_s \vec{v}_s\right) = -\varepsilon_g \nabla.P_g + \nabla.\overline{\overline{\tau_s}} - \nabla.P_s + \varepsilon_s \rho_s \vec{g} + S_s \tag{9}$$

Momentum equation (gas phase and solid phase) [38]

$$\frac{\partial}{\partial_t}\left(\varepsilon_g \rho_g H_g\right) + \nabla.\left(\varepsilon_g \rho_g \vec{v}_g H_g\right) = \nabla.\left(k_i \nabla.T_g\right) + S_h \tag{10}$$

(Energy equation) [38, 39]

$$\varepsilon_g + \varepsilon_s = 1 \tag{11}$$

(Phase volume fraction) [40]

$$\rho_s = \left(1 - \varepsilon_o\right) + \varepsilon_0.\rho_g \tag{12}$$

(Suspension density) [41]

The phase volume fraction "ε" sums the gas and solid phases to unity. The heat energy liberated during any chemical reaction is denoted by the source term "S_h" in Eq. 10. The correlation for particle suspension density is depicted in Eq. 12. The suspension density is proportional to the fluid velocity at lower velocity. However, at higher velocities, the fluid behaviour becomes vigorous leading to the fast escape of solid particles that abruptly reduces the suspension rate. The bed voidage or gap between the particles is also proportional to the fluid velocity.

Results and discussion

Static temperature

With air preheating

The variation of DTBFBR operating temperature for Phase-2 and Phase-1 along the axial direction with air preheating is plotted in Figs. 3 and 4. In both cases, it is observed that the preheating causes to maintaining the temperature almost steady inside the reactor, which would improve the thermal breakdown of solid biomass particles. Although inlet temperature is 333K (summing preheat 60°), the particle temperature of 100 μm drops to an average of 315 K due to fluid flow and remains unvaried towards the reactor exit.

The temperature at the heating region (patched between 0.4 and 0.6 m) is 973 K for the particle size 100 μm, whereas in the case of 300 μm at fluid velocity of 2m/s, the temperature of both the solid and gas phase is witnessed to be constant although heating region temperature is 1073 K. The temperature drop inside the reactor core might be due to the reactor not being insulated during the simulation. The 800 μm particle having heating zone temperature of 1173K shows the highest net temperature of 353 K, with core temperature 345 K and maximum outlet temperature of 350K. Figure 3 shows a constant temperature pattern for all the particle sizes due to preheating of the gasifying agent. However, in Fig. 4, the Phase-2 temperature is not constant due to increased particle suspension density and fluid velocity that causes vigorous particle flow push towards the exit.
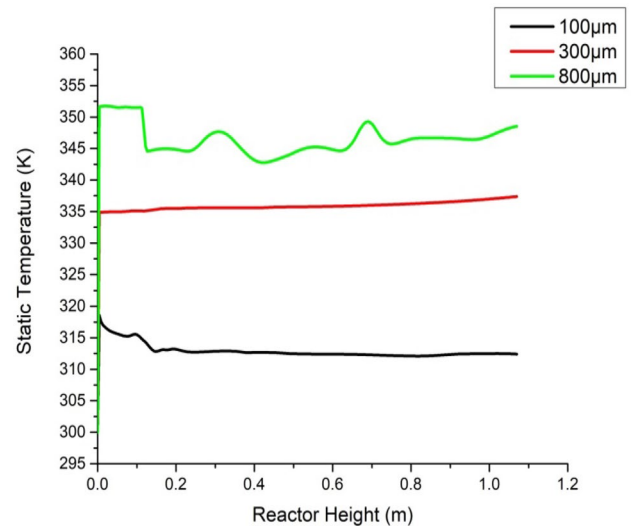

Fig. 4 Plot for static temperature variation along the axial height of DTBFBR with preheating (60 ℃) for Phase-2 wood biomass having particle sizes 100,300,800 μm

The solid temperature (800 μm) is seen to be varying with higher fluid velocity, but the temperature distribution inside the reactor is observed to be uniform under lower velocities for 100and 300 μm particle sizes.

Without air preheating

Figures 5 and 6 noticeably highlight the temperature variation of wood biomass particles without using air preheating. Though it is observed that there is no significant temperature rise inside the reactor, the Phase-2 particles show a temperature drop of almost 60K from the initial
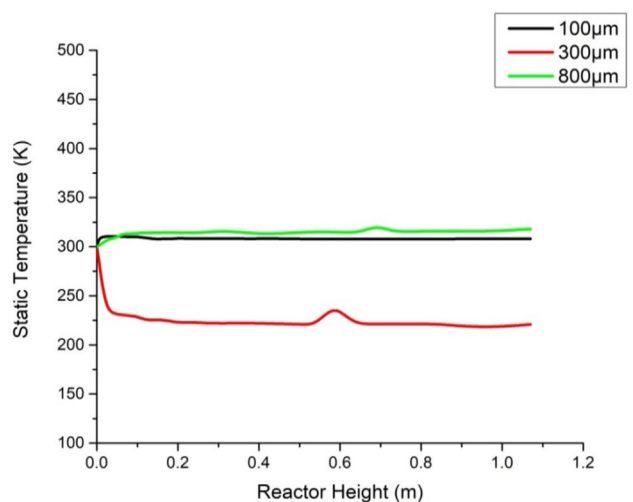

Fig. 3 Plot for static temperature variation along the axial height of DTBFBR with preheating (60 ℃) for Phase-1 air with inlet velocity 1, 2, 3 m/s

Fig. 5 Plot for static temperature variation along the axial height of DTBFBR without preheating of Phase-1 air with inlet velocity 1, 2, 3 m/s
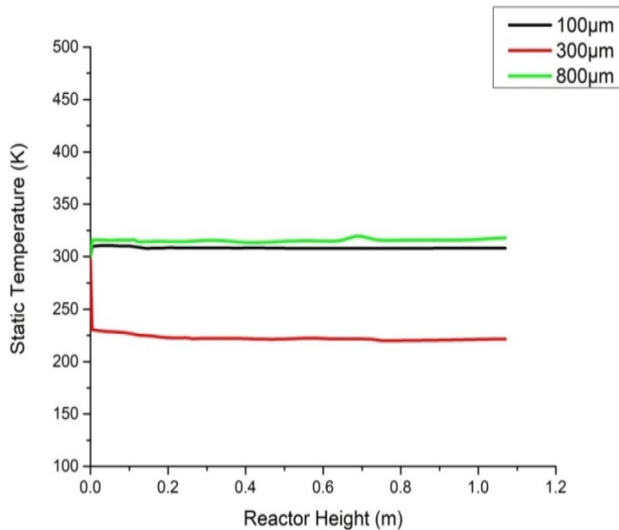
Fig. 6 Plot for static temperature variation along the axial height of DTBFBR without preheating for Phase-2 wood biomass having particle sizes 100, 300, 800 μm

temperature of 300 K when compared with the case of preheating. The Phase-2 particles undergoing no preheating report lower temperature inside the reactor that may reduce the overall temperature required for species transformation of solid wood biomass particles.

Static pressure

With air preheating

The pressure value at the inlet is set to the atmospheric pressure value of 101325 Pa; the pressure drop inside the reactor for Phase-1 is recorded in Fig. 7 and Phase-2 in Fig. 8. In both cases, it is observed that the pressure drop is sharp except for 100 μm with low fluid velocity. In Fig. 8, the particle trajectory is also plotted. Since the DTBFBR has enough cross-sectional area and the particles being smaller in size, the fluidizing agent easily lifts the particles with it. As the fluid velocity increases from unity, in case of 300 μm and 800 μm, the particles are blown up rapidly with the incoming air towards the reactor, which reduces the pressure inside DTBFBR. Hence, for the effective thermal and chemical breakdown of the solid biomass particles [42], the reactor pressure (>1 atm) coupled with gasification zone temperature (>900 ℃) needs to be maintained to higher values as discussed in studies [43, 44]. This increase in pressure and gasification temperature ensures better syngas production with enriched constituents and tar cracking as highlighted in similar works over biomass [45].
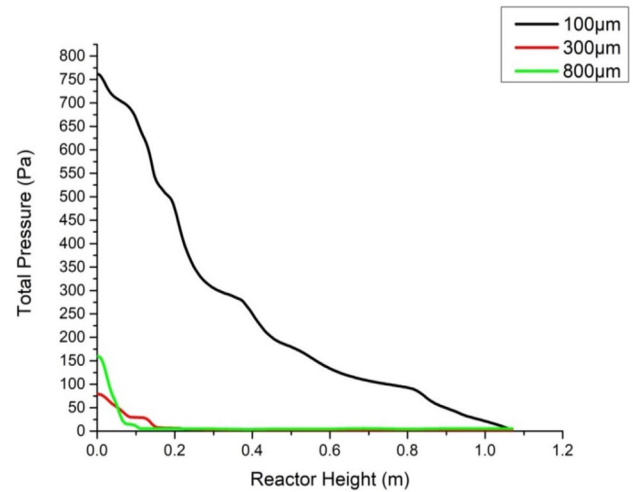

Fig. 7 Plot for total pressure variation along the axial height of DTB-FBR with preheating (60 ℃) of Phase-1 air with inlet velocity 1, 2, 3 m/s

Without air preheating

The variation of total pressure for Phase-1 and Phase-2 is detailed in Figs. 9 and 10. However, compared to the case of air preheated simulation curves in Figs. 7 and 8, no prominent variation is seen for the case without air preheating. The particles are easily lifted towards the exit with incoming fluidizing agent under varied velocities. Under lower air velocities, particles remaining within the reactor are observed to be more as plotted in Fig. 10 for 100 μm. The increased Phase-1 velocity is detected to diminish the overall acting pressure inside the DTBFBR as plotted in Fig. 9. However, an increase in total pressure will enhance the gasification process.
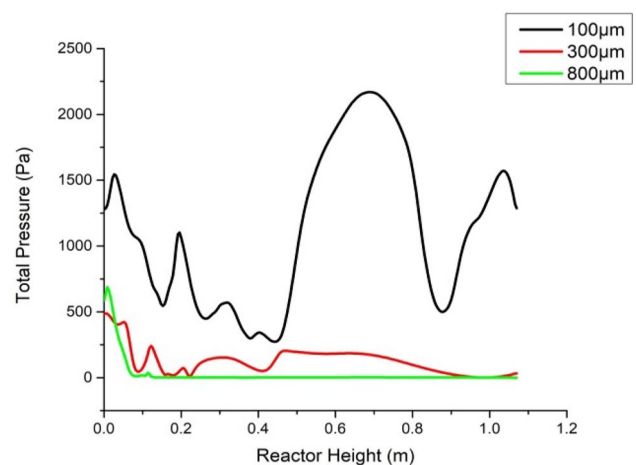

Fig. 8 Plot for total pressure variation along the axial height of DTB-FBR with preheating (60℃) for Phase-2 wood biomass having particle sizes 100, 300, 800 μm
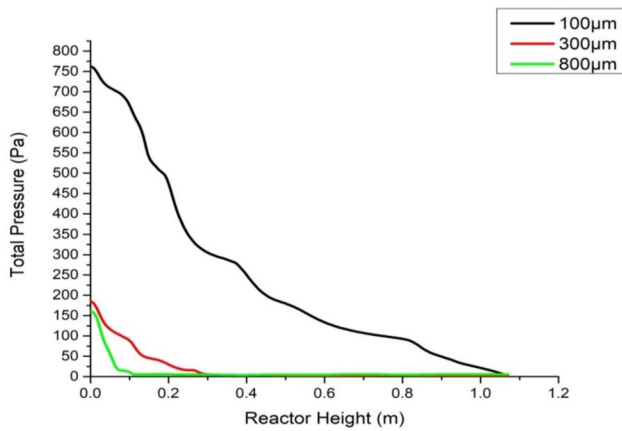
Fig. 9 Plot for total pressure variation along the axial height of DTB-FBR without preheating of Phase-1 air with inlet velocity 1, 2, 3 m/s
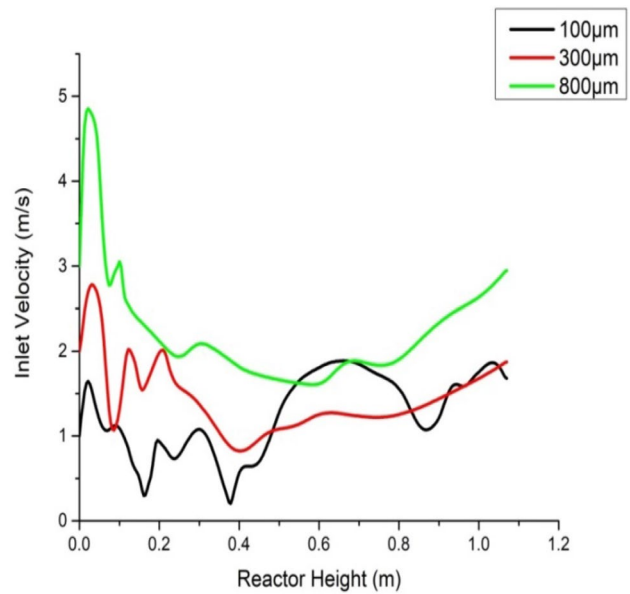

Fig. 11 Plot for variation of airflow velocity along the axial height of DTBFBR with preheating (60℃) for Phase-1 with inlet velocity 1, 2, 3 m/s
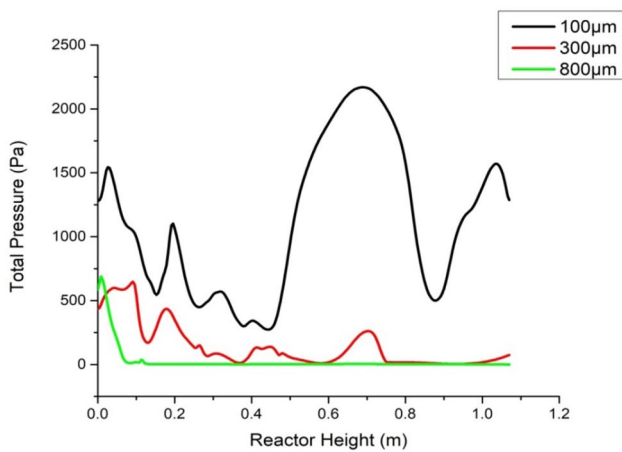

Fig. 10 Plot for total pressure variation along the axial height of DTBFBR without preheating; Phase-2 wood biomass having particle sizes 100, 300, 800 μm

Fig. 12 Plot for variation of airflow velocity along the axial height of DTBFBR with preheating (60 ℃) for Phase-2 wood biomass having particle sizes 100, 300, 800 μm

Inlet velocity

With air preheating

The velocity profile of gasifying agent, air, is plotted in Fig. 11. The flow profile is seen to be stabilized after the initial particle push upward, and less vibrant nature is attained after the reactor heating zone. However, in Fig. 12, the solid velocity of 100 μm is increased above the fluid velocity of 1m/s from the inlet. The retention time of particles inside the reactor is observed to be good under low fluid velocities. However, the prolonged operation of reactor under lower
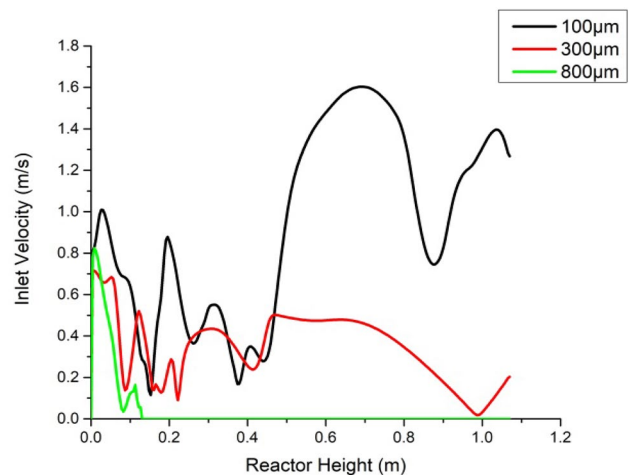
velocities might cause the particles to retain inside the reactor leading to incomplete combustion and agglomeration. Hence, optimum air velocity and particle size can provide good retention time coupled with particle suspension density that improves the process characteristics. As the particle size becomes smaller, the drag force exerted by the fluid easily
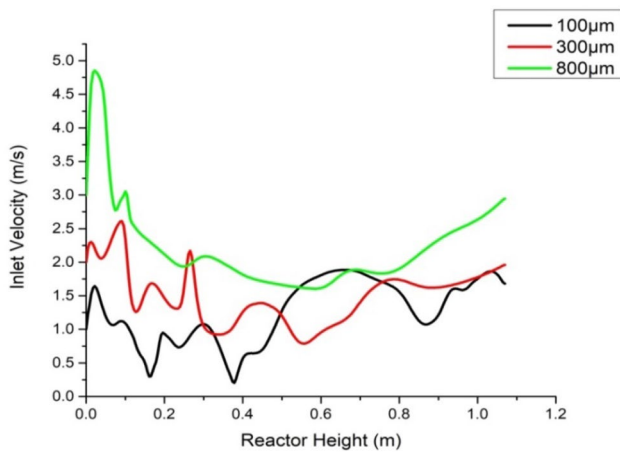
Fig. 13 Plot for variation of airflow velocity along the axial height of DTBFBR without preheating for Phase-1 with inlet velocity 1, 2, 3 m/s
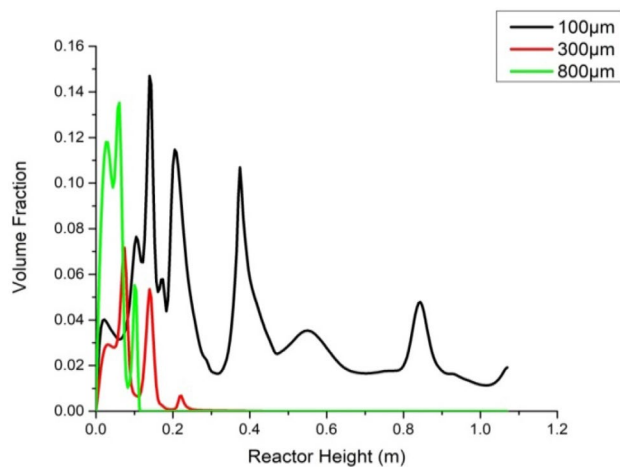

Fig. 15 Plot for variation of volume fraction along the axial height of DTBFBR with preheating (60 ℃) for Phase-2 wood biomass having particle sizes 100, 300, 800 μm and inlet velocity 1, 2, 3 m/s

Fig. 14 Plot for variation of airflow velocity along the axial height of DTBFBR without preheating for Phase-2 wood biomass having particle sizes 100, 300, 800 μm

Fig. 16 Plot for variation of volume fraction along the axial height of DTBFBR without preheating for Phase-2 wood biomass having particle sizes 100, 300, 800 μm and inlet velocity 1, 2, 3 m/s

carries up the solid particles with it, whereas for increased particle size more drag force is to be imparted as inferred from Figs. 11 and 12.

Without air preheating

On comparing the above plots (Figs. 13 and 14) with the plots for airflow velocity variation in the case of preheating (Figs. 11 and 12), no significant variation is found. The effect of air preheating has not made any substantial variation in the overall velocity of both Phase-1 and Phase 2.
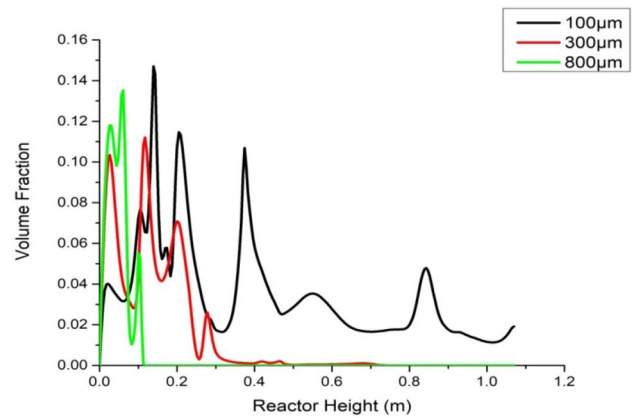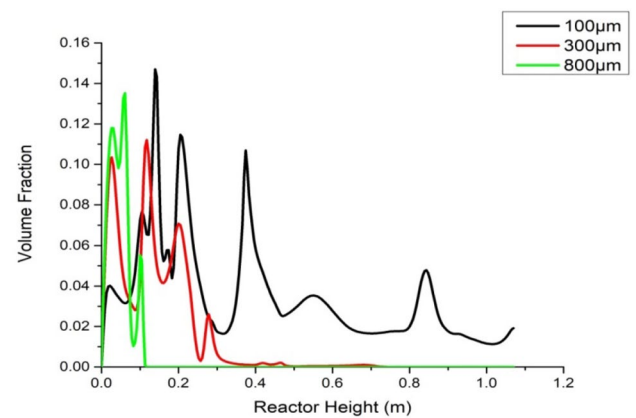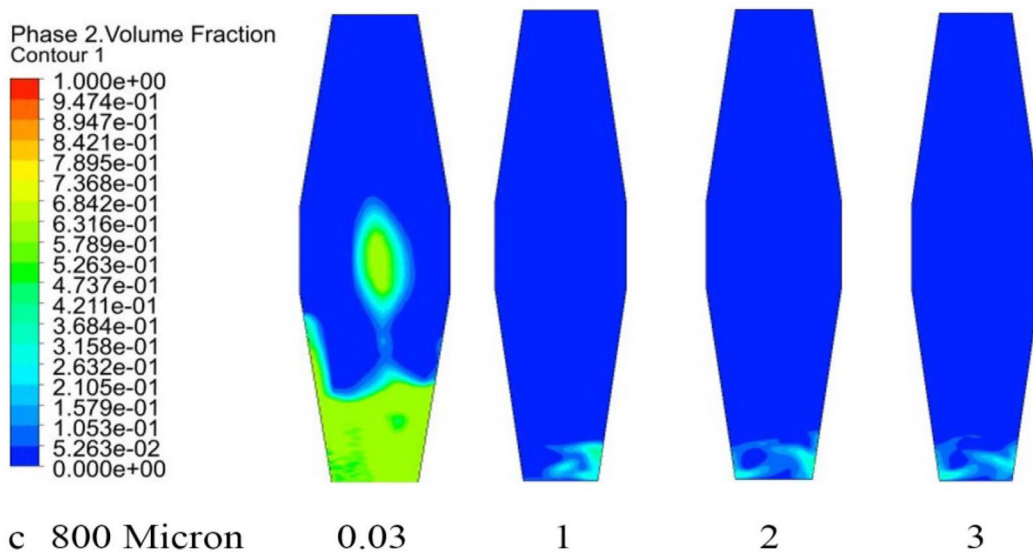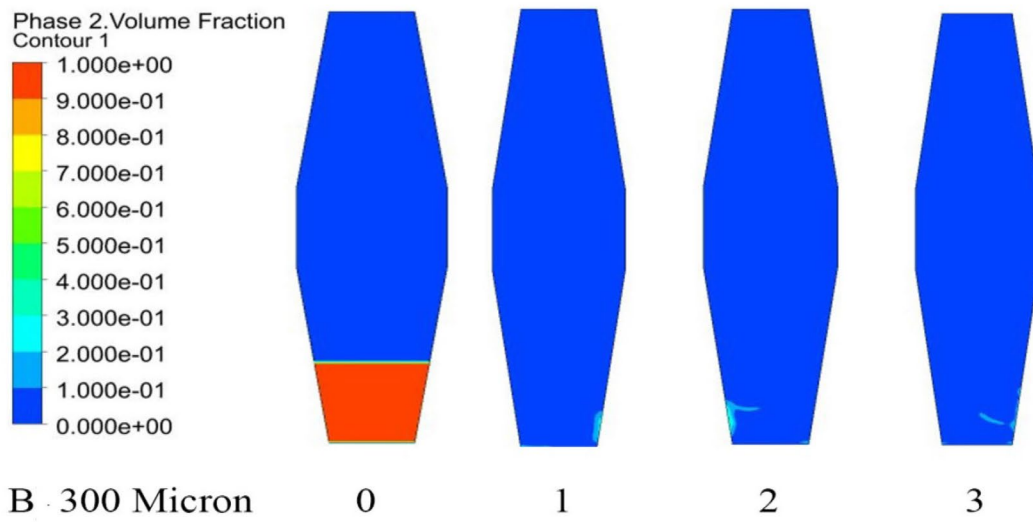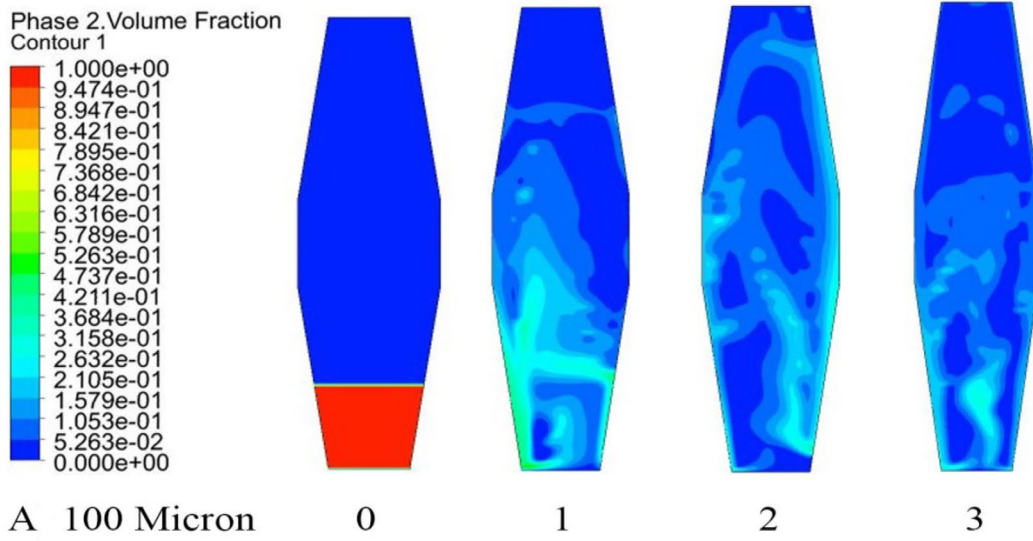
Volume fraction

The correlation for volume fraction is depicted in Eq. 11, where the sum of solid and gas phase equals unity. The wood biomass region is patched up to 0.20 m. Figure 15 illustrates the need for optimized inlet fluid velocity for better gasification performance in DTBFBR. Except for 100 μm, the volume fraction of 300 and 800 μm particle size at the heating region (between 0.4 and 0.6 m from inlet) falls to zero. It means that higher the velocity, higher will be the blown-out rate of particles from the reactor, which causes poor gasification performance. Hence, it is required to maintain the solid velocity so as to improve the reaction time and solid to

A 100 Micron   0   1   2   3

B 300 Micron   0   1   2   3

c 800 Micron   0.03   1   2   3

◄**Fig. 17** Plot for variation of volume fraction along with the axial height of DTBFBR with time (seconds) for Phase-2 wood biomass with preheating having particle sizes 100, 300, 800 μm

gas transformation. The presence of 300 μm particles in the reactor heating zone is slightly more compared to the case with preheating as shown in Fig. 16. This may be due to the low-temperature build-up in the reactor that cannot aid in solid–gas conversion. This scenario of particles being blown out at higher velocity is clearly illustrated with simulation results in Figs. 17 and 18.

Although preheating causes to maintain the reactor temperature, the reactor operation at higher air velocities is not desirable as it would lead to incomplete combustion and low solid–gas conversion efficiencies. The solid particle movement is grasped in Fig. 17A and 18A for 100microns where the particles are lifted towards the exit after undergoing thermal degradation, and thus, solid volume fraction is reduced, whereas in Fig. 17B, C, Fig. 18B and C, the wood biomass having particle size 300 and 800 μm is found only in traces in the reactor as they are blown out with the Phase-1 air.

Taper angle

From the results obtained the tapered bottom of DTBFBR shows that the pressure drop increases with taper angle at first but limited to higher taper angle variations. This result has not been contradicted when compared with the previous works conducted [46]. The increase in taper angle of the reactor causes the solid bed to partially fluidize, and blown-out rate is seen to be partial. The effect of pressure drop on the utility of various reactor taper angles with inlet fluid velocity is portrayed in Fig. 19.

The comparison of various particle sizes and pressure drop upon inlet velocity obtained from various studies [27, 38, 46] is plotted for validating the work. The pressure drop becomes higher at increased fluid velocity and declines with the particle concentration inside the DTBFR due to conversion reactions. It is also observed in Fig. 19 that the pressure drop decreases with increase in particle sizes. However, compared to other tapered reactors, DTBFBR shows better results in terms of increased pressure values that will evidently enhance the gasification operations. The DTBFBR

design with a taper angle of 5° is novel and has not been discussed elsewhere. The taper angle of the reactor provides enough velocity gradient, particle suspension density and solid circulation that can improve the chemical reaction processes. However, with increased taper angles, the pressure drop also increases. The available studies purely discuss either columnar reactor or tapered-in reactor with various taper angles. Since better experimental work is not available with the present case, simulation study has been pursued with the available literature data to portray the prospects in using DTBFBR.

Conclusions

The variation of process parameters in a DTBFBR with solid wood biomass material using preheated/non-preheated air has been successfully studied, and the results are obtained. Here, the biomass particle size of 100μm exhibits better results when compared to 300and 800 μm. The simulations with non-preheated air portray the temperature fall inside the DTBFBR that reduces the overall temperature required for the thermal breakdown of solid biomass sizes. In both cases, the reduction of temperature in the heating zone might be due to the reactor being heated up externally. The variation of volume fraction for both the cases of air with and without preheating of 60° shows no significant variation, except for 300 μm, with preheating where the volume fraction falls to zero at the heating zone between 0.4 and 0.6 m. This may either be due to solid–gas conversion or phase change of the particles. The double-tapered reactor design has good inner volume that possibly benefits the suspension density, pressure and solid circulation that enhances the solid–gas conversion ability. This makes the DTBFBR unique over cylindrical-shaped reactors. The present study only discusses the parametric study of mentioned biomass particle size in DTBFBR. The reactor performance using preheated air is found to be very good compared to the case with non-preheated air. Finally, producing energy from biomass sources through thermochemical conversion route is a viable alternative to diminish the adverse environmental impacts.
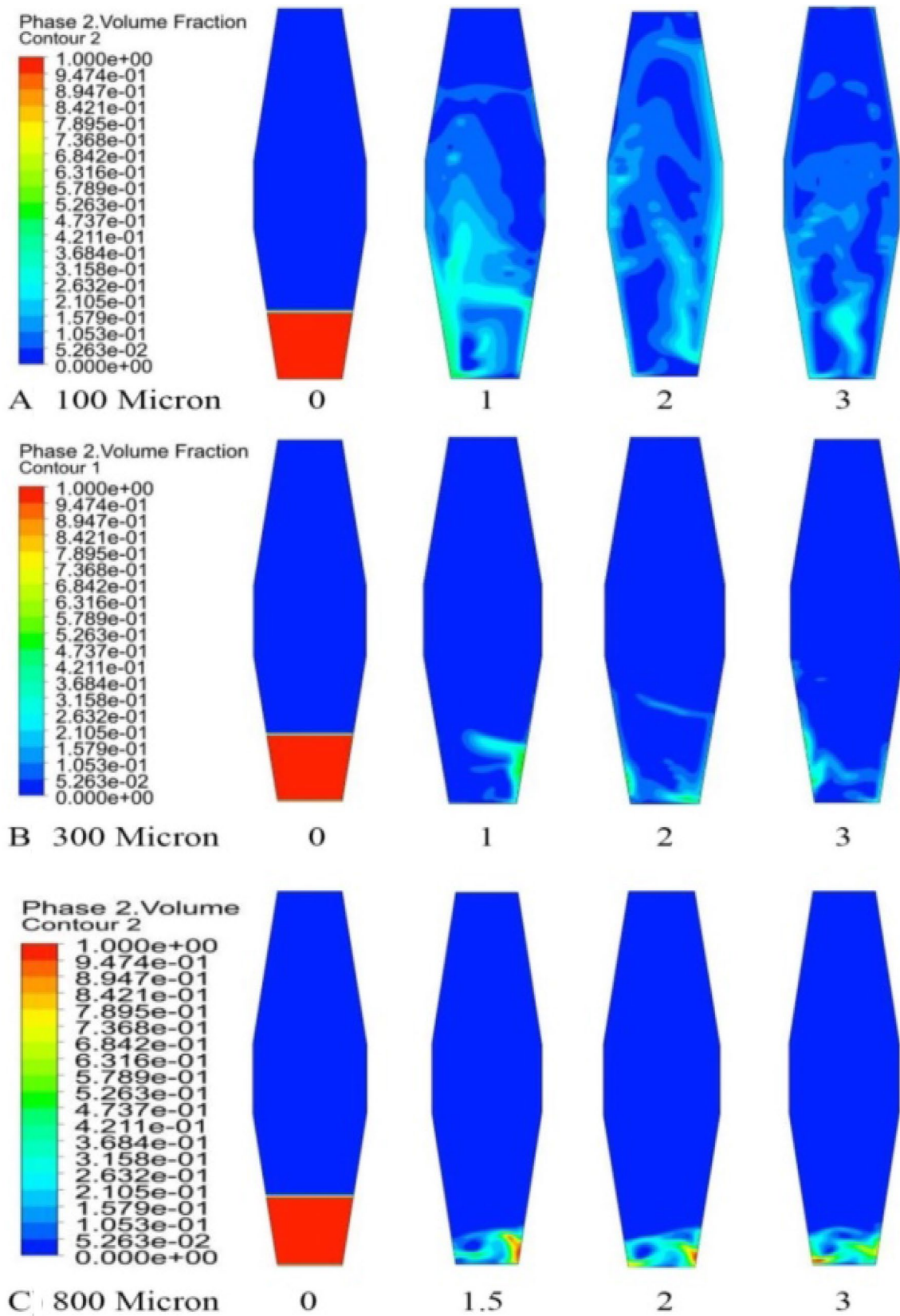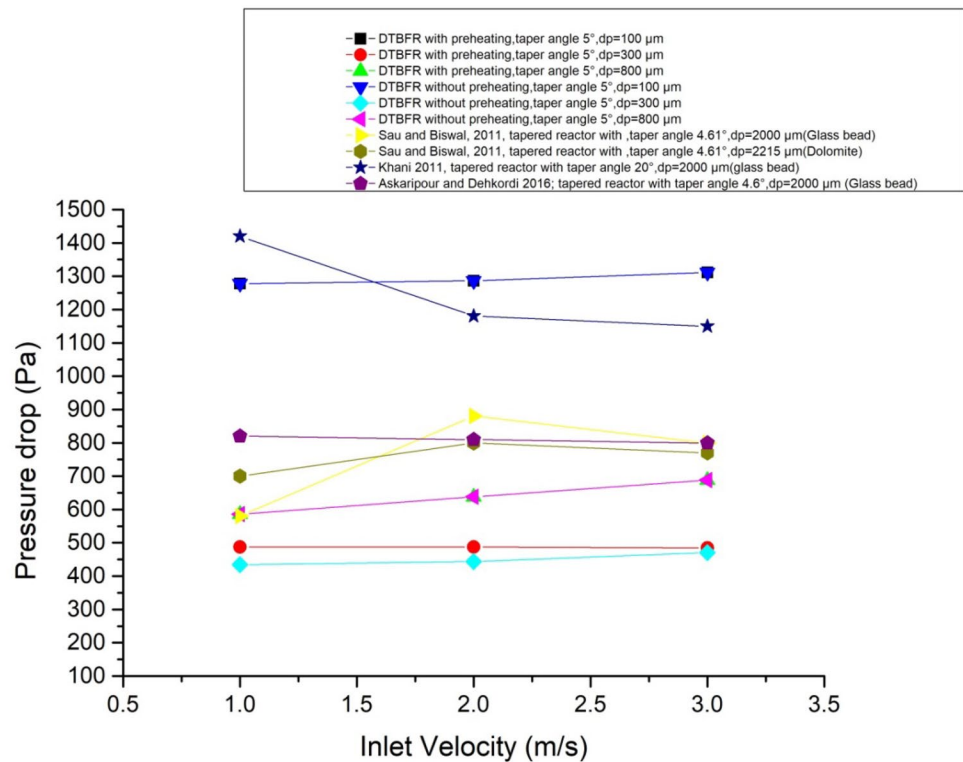
Fig. 18 Plot for variation of volume fraction along with the axial height of DTBFBR with time (seconds) for Phase-2 wood biomass without pre-heating having particle sizes 100, 300, 800 μm

Fig. 19 Plot for pressure drop against Inlet velocity for various reactor taper angles and particle sizes

Declarations

Conflict of interest On behalf of all authors, the corresponding author states that there is no conflict of interest.

References

1. Sansaniwal, S.K., Pal, K., Rosen, M.A., Tyagi, S.K.: Recent advances in the development of biomass gasi fi cation technology : a comprehensive review. Renew. Sustain. Energy Rev. **72**, 363–384 (2017). https://doi.org/10.1016/j.rser.2017.01.038
2. Heidenreich, S., Foscolo, P.U.: New concepts in biomass gasification. Prog. Energy Combust. Sci. **46**, 72–95 (2015). https://doi.org/10.1016/j.pecs.2014.06.002
3. Kundu, K., Chatterjee, A., Bhattacharyya, T.: Thermochemical Conversion of Biomass to Bioenergy : A Review. (2018)
4. Puig-arnavat, M., Bruno, J.C., Coronas, A.: Review and analysis of biomass gasification models. Renew. Sustain. Energy Rev. **14**, 2841–2851 (2010). https://doi.org/10.1016/j.rser.2010.07.030
5. Kaltschmitt, M.: Biomass as Renewable Source of Energy : Possible Conversion Routes. (2019)
6. Atnaw, S.M., Sulaiman, S.A., Yusup, S.: Biomass gasification. Springer, Cham (2017)
7. Klemm, M.: Small scale biomass gasification for rural electrification. Springer, New York (2019)
8. Sau, D.C., Biswal, K.C.: Computational fluid dynamics and experimental study of the hydrodynamics of a gas – solid tapered fluidized bed. Appl. Math. Model. **35**, 2265–2278 (2011). https://doi.org/10.1016/j.apm.2010.11.037
9. Rasteh, M., Farhadi, F., Bahramian, A.: Hydrodynamic characteristics of gas – solid tapered fl uidized beds : experimental studies and empirical models. Powder Technol. **283**, 355–367 (2015). https://doi.org/10.1016/j.powtec.2015.06.002
10. Schulzke, T.: Biomass gasification : conversion of forest residues into heat, electricity and base chemicals. Chem. Pap. **73**, 1833–1852 (2019). https://doi.org/10.1007/s11696-019-00801-1
11. Pattanayak, S., Hauchhum, L., Loha, C., Sailo, L., Mishra, L.: Experimental investigation on pyrolysis kinetics, reaction mechanisms and thermodynamic parameters of biomass and tar in N2 atmosphere. Sustain. Energy Technol. Assessments. **48**, 101632 (2021). https://doi.org/10.1016/j.seta.2021.101632
12. Pattanayak, S., Hauchhum, L., Loha, C., Sailo, L.: Selection criteria of appropriate bamboo based biomass for thermochemical conversion process. Biomass Convers. Biorefinery. **10**, 401–407 (2020). https://doi.org/10.1007/s13399-019-00421-5
13. Wu, K.T., Chein, R.Y.: Modeling of biomass gasification with preheated air at high temperatures. Energy Procedia **75**, 214–219 (2015). https://doi.org/10.1016/j.egypro.2015.07.307
14. Kalita, P., Baruah, D.: Investigation of biomass gasi fi er product gas composition and its characterization. Springer, Singapore (2018)
15. Mallick, D., Buragohain, B., Mahanta, P.: Gasi fi cation of Mixed Biomass : Analysis Using Equilibrium , Semi-equilibrium , and Kinetic Models. 223–241 (2018)
16. Tavares, R., Monteiro, E., Tabet, F., Rouboa, A.: Numerical investigation of optimum operating conditions for syngas and hydrogen production from biomass gasi fi cation using Aspen Plus. Renew. Energy. **146**, 1309–1314 (2020). https://doi.org/10.1016/j.renene.2019.07.051
17. Zhang, Z., Pang, S.: Experimental investigation of biomass devolatilization in steam gasification in a dual fluidised bed gasifier. Fuel. **188**, 628–635 (2017). https://doi.org/10.1016/j.fuel.2016.10.074
18. Watson, J., Zhang, Y., Si, B., Chen, W., Souza, R.. De.: Gasi fi cation of biowaste : a critical review and outlooks. Renew. Sustain.

Energy Rev. **83**, 1–17 (2018). https://doi.org/10.1016/j.rser.2017.10.003

19. Sharma, S., Sheth, P.N.: Air – steam biomass gasification : experiments, modeling and simulation. Energy Convers. Manag. **110**, 307–318 (2016). https://doi.org/10.1016/j.enconman.2015.12.030

20. Doherty, W., Reynolds, A., Kennedy, D.: The effect of air preheating in a biomass CFB gasifier using ASPEN plus simulation the effect of air preheating in a biomass CFB gasifier using ASPEN plus simulation. Biomass Bioenergy (2009). https://doi.org/10.1016/j.biombioe.2009.05.004.This

21. Qi, T., Lei, T., Yan, B., Chen, G.: ScienceDirect Biomass steam gasification in bubbling fluidized bed for higher-H 2 syngas : CFD simulation with coarse grain model. Int. J. Hydrogen Energy. **44**, 6448–6460 (2019). https://doi.org/10.1016/j.ijhydene.2019.01.146

22. Kalita, P., Saha, U.K., Mahanta, P.: Effect of biomass blending on hydrodynamics and heat transfer behavior in a pressurized circulating fluidized bed unit. Int. J. Heat Mass Transf. **60**, 531–541 (2013). https://doi.org/10.1016/j.ijheatmasstransfer.2013.01.043

23. Kalita, P., Saha, U.K., Mahanta, P.: Parametric study on the hydrodynamics and heat transfer along the riser of a pressurized circulating fluidized bed unit. Exp. Therm. Fluid Sci. **44**, 620–630 (2013). https://doi.org/10.1016/j.expthermflusci.2012.09.001

24. Kalita, P., Mahanta, P., Saha, U.K.: Some studies on wall-to-bed heat transfer in a pressurized circulating fluidized bed unit. Procedia Eng. **56**, 163–172 (2013). https://doi.org/10.1016/j.proeng.2013.03.103

25. Khan, M.S., Mitra, S., Ghatage, S.V., Doroodchi, E., Joshi, J.B., Evans, G.M.: Segregation and dispersion studies in binary solid-liquid fluidised beds: a theoretical and computational study. Powder Technol. **314**, 400–411 (2017). https://doi.org/10.1016/j.powtec.2016.12.070

26. Stendardo, S., Ugo, P., Nobili, M., Scaccia, S.: High quality syngas production via steam-oxygen blown bubbling fluidised bed gasifier. Energy **103**, 697 (2016). https://doi.org/10.1016/j.energy.2016.03.011

27. Sau, D.C., Biswal, K.C.: Computational fluid dynamics and experimental study of the hydrodynamics of a gas-solid tapered fluidized bed. Appl. Math. Model. **35**, 2265–2278 (2011). https://doi.org/10.1016/j.apm.2010.11.037

28. Duangkhamchan, W., Ronsse, F., Depypere, F., Dewettinck, K., Pieters, J.G.: Comparison and evaluation of interphase momentum exchange models for simulation of the solids volume fraction in tapered fluidised beds. Chem. Eng. Sci. **65**, 3100–3112 (2010). https://doi.org/10.1016/j.ces.2010.02.008

29. Gopan, G., Hauchhum, L., Kalita, P.,Pattanayak, S., Parametric study of tapered fluidized bed reactor under varied taper angle using TFM Parametric Study of Tapered Fluidized Bed Reactor Under Varied Taper Angle Using TFM. 020020, (2021)

30. Fuchs, J.: The impact of gasification temperature on the process characteristics of sorption enhanced reforming of biomass. Biomass. Conv. Bioref. **10**, 925 (2019)

31. Campoy, M., Gómez-Barea, A., Ollero, P., Nilsson, S.: Gasification of wastes in a pilot fluidized bed gasifier. Fuel Process. Technol. **121**, 63–69 (2014). https://doi.org/10.1016/j.fuproc.2013.12.019

32. Pjontek, D., Macchi, A.: Hydrodynamic comparison of spherical and cylindrical particles in a gas-liquid-solid fluidized bed at elevated pressure and high gas holdup conditions. Powder Technol.

253, 657–676 (2014). https://doi.org/10.1016/j.powtec.2013.12.030

33. Ku, X., Jin, H., Lin, J.: Comparison of gasification performances between raw and torrefied biomasses in an air-blown fluidized-bed gasifier. Chem. Eng. Sci. **168**, 235–249 (2017). https://doi.org/10.1016/j.ces.2017.04.050

34. Wojnicka, B.: Modelling of biomass gasification with steam. Biomass Conv Bioref **11**, 1787 (2019)

35. Gómez-Barea, A., Leckner, B.: Modeling of biomass gasification in fluidized bed. Prog. Energy Combust. Sci. **36**, 444–509 (2010). https://doi.org/10.1016/j.pecs.2009.12.002

36. Huang, Z., Zhang, J., Zhao, Y., Zhang, H., Yue, G.: Kinetic studies of char gasi fi cation by steam and CO 2 in the presence of H 2 and CO. Fuel Process. Technol. **91**, 843–847 (2010). https://doi.org/10.1016/j.fuproc.2009.12.020

37. Kaushal, P., Abedi, J., Mahinpey, N.: A comprehensive mathematical model for biomass gasification in a bubbling fluidized bed reactor. Fuel. **89**, 3650–3661 (2010). https://doi.org/10.1016/j.fuel.2010.07.036

38. Askaripour, H., Dehkordi, A.M.: Effects of initial static bed height on fractional conversion and bed pressure drop in tapered-in and tapered-out fluidized bed reactors. Int. J. Multiphase Flow **79**, 50–61 (2016). https://doi.org/10.1016/j.ijmultiphaseflow.2015.08.006

39. Chen, L., Yang, X., Li, G., Li, X., Snape, C.: Prediction of bubble fluidisation during chemical looping combustion using CFD simulation. Comput. Chem. Eng. **99**, 82–95 (2017). https://doi.org/10.1016/j.compchemeng.2017.01.009

40. Ranganathan, P., Gu, S.: Computational fluid dynamics modelling of biomass fast pyrolysis in fluidised bed reactors, focusing different kinetic schemes. Bioresour. Technol. **213**, 333–341 (2015). https://doi.org/10.1016/j.biortech.2016.02.042

41. Prins, M.J.: Thermodynamic analysis of biomass gasification and torrefaction. (2005)

42. Di Natale, F., Nigro, R.: An experimental procedure to estimate tube erosion rates in bubbling fluidised beds. Powder Technol. **287**, 96–107 (2016). https://doi.org/10.1016/j.powtec.2015.10.001

43. Mirmoshtaghi, G., Li, H., Thorin, E., Dahlquist, E.: Evaluation of different biomass gasification modeling approaches for fluidized bed gasifiers. Biomass and Bioenergy. **91**, 69–82 (2016). https://doi.org/10.1016/j.biombioe.2016.05.002

44. Feng, F., Song, G., Shen, L., Xiao, J.: Simulation of bio-syngas production from biomass gasification via pressurized interconnected fluidized beds. (2014). doi: https://doi.org/10.1007/978-3-642-37922-2

45. Thakkar, M., Mohanty, P., Shah, M., Singh, V.: An Overview of Biomass Gasification. 147–176

46. Khani, M.H.: Models for prediction of hydrodynamic characteristics of gas – solid tapered and mini-tapered fl uidized beds. Powder Technol. **205**, 224–230 (2011). https://doi.org/10.1016/j.powtec.2010.09.018